The Journal of Chemical Physics

Solvation dynamics in electronically polarizable solvents: Theoretical treatment using solvent-polarizable three-dimensional reference interaction-site model theory combined with time-dependent density functional theory

Cite as: J. Chem. Phys. **154**, 044504 (2021); https://doi.org/10.1063/5.0036289
Submitted: 03 November 2020 • Accepted: 18 December 2020 • Published Online: 29 January 2021

Tsuyoshi Yamaguchi and Norio Yoshida

The Journal of Chemical Physics ARTICLE scitation.org/journal/jcp

Solvation dynamics in electronically polarizable solvents: Theoretical treatment using solvent-polarizable three-dimensional reference interaction-site model theory combined with time-dependent density functional theory

Cite as: J. Chem. Phys. 154, 044504 (2021); doi: 10.1063/5.0036289
Submitted: 3 November 2020 • Accepted: 18 December 2020 •
Published Online: 29 January 2021

Tsuyoshi Yamaguchi[1,a)] and Norio Yoshida[2,a)]

AFFILIATIONS

[1]Graduate School of Engineering, Nagoya University, Chikusa, Nagoya 464–8603, Japan
[2]Department of Chemistry, Graduate School of Science, Kyushu University, 744 Motooka, Nishiku, Fukuoka 819-0395, Japan

[a)]**Authors to whom correspondence should be addressed:** yamaguchi.tsuyoshi@material.nagoya-u.ac.jp and noriwo@chem.kyushu-univ.jp

ABSTRACT

The theory of solvation structure in an electronically polarizable solvent recently proposed by us, referred to as the "solvent-polarizable three-dimensional reference interaction-site model theory," is extended to dynamics in this study through the combination with time-dependent density functional theory. Test calculations are performed on model charge-transfer systems in water, and the effects of electronic polarizability on solvation dynamics are examined. The electronic polarizability slightly retards the solvation dynamics. This is ascribed to the decrease in the curvature of the nonequilibrium free energy profile along the solvation coordinate. The solvent relaxation is bimodal, and the faster and the slower modes are assigned to the reorientational and the translational modes, respectively, as was already reported by the surrogate theory combined with the site–site Smoluchowski–Vlasov equation. The relaxation path along the solvation coordinate is a little higher than the minimum free energy path because the translational mode is fixed in the time scale of the reorientational relaxation.

I. INTRODUCTION

Chemical processes in solution proceed under both static and dynamic effects of solvents. Static solvent effects refer to the thermodynamic stabilization of the solute in solution through the solute–solvent interaction, and the dynamic solvent effects are related to the time profile of the solute–solvent interaction. An understanding of the latter is particularly important in diffusion, charge-transfer reactions, and isomerization reactions.

The dynamics of the solute–solvent interaction can be accessed experimentally through the measurement of solvation dynamics.[1–6] In solvation dynamics, the solute possesses two states: the ground and the excited states. The solute–solvent interactions in the two states differ from each other, and the transition energy between these two states depends on the instantaneous configuration of solvent molecules around the solute. The equilibrium solvation structures of the two states also differ. After a sudden change in the state of the solute, therefore, the solvation structure relaxes to the equilibrium solvation of the final state, and the transition

energy between these two states also relaxes. Even in equilibrium, the transition energy fluctuates around its average value due to the thermal motion of the surrounding solvent molecules. The response of the transition energy to the change in the solute state is related to the thermal fluctuation of the transition energy as per the linear response theory, and both are referred to as "solvation dynamics."

When the ground and the excited states correspond to the product and the reactant states of the charge-transfer reaction, the solvation dynamics is regarded as the dynamics of the solvation coordinate, which plays a crucial role in determining the reaction rate. The charge-transfer reaction in polar solvents is strongly coupled to the thermal fluctuation of the solvent, and the rate at which the solvation structure changes to the configuration favorable to the charge transfer is one of the important factors in determining the overall rate constant. In polar solvation dynamics, where the dipole moment of the solute changes upon transition between the two states, the solvation dynamics is also related to the dielectric friction on the translational diffusion of ions.[6]

Due to the importance of solvation dynamics, as described above, numerous experimental studies on solvation dynamics in solution have been carried out. Most include the use of pulsed lasers, and a variety of experimental studies have been applied, including fluorescence dynamic Stokes shift,[4,5,7] transient hole-burning spectroscopy,[8] and photon echo,[9] among others.

The solvation dynamics has also been targeted by various levels of computational modeling.[3] The simplest one is the dielectric continuum model in which the response of the surrounding solvent molecules is approximated as that of the dielectric material whose frequency-dependent dielectric permittivity is characterized by that of the bulk solvent.[4,5] At the other extreme, fully atomistic molecular dynamics (MD) simulation has also been applied to solvation dynamics.[10,11]

Distribution function theories are important theories in that they can provide a microscopic picture of solvation, handling only the limited number of degrees of freedom of solvent molecules. The distribution function theories were originally developed for equilibrium properties, where the equilibrium solvation structure and the thermodynamic properties are calculated from the molecular structure and the intermolecular interaction by solving a set of integral equations.[12] One of the representative distribution function theories is the three-dimensional reference interaction-site model (3D-RISM) theory, which has been applied to various systems, ranging from small molecules to proteins in water.[13] The extension of the distribution function theory to solvation dynamics has been roughly classified in two different ways. The first one is the surrogate theory, which approximates the dynamics of solvent molecules around the solute in terms of the intermediate scattering functions of the bulk solvent by introducing the surrogate Hamiltonian that linearly interpolates the initial and the final states.[14–16] The second one is the time-dependent density functional theory (TDDFT) in which the dynamics of the solvation structure is related to the functional derivative of the free energy with respect to the density field of the solvent.[17–19] An advantage of the latter is that it can include some kinds of nonlinearity, whereas the former is an essentially linearized theory.

In a series of our studies, we have developed the solvent-polarizable 3D-RISM (sp-3D-RISM) theory, which extends the conventional 3D-RISM theory to include the electronic polarizability of solvent molecules.[20,21] Our intention in developing this novel theory is to treat the charge-transfer reaction in solvents, where electrostatic interaction between the charge distribution of the solute and the dipole moments (including both permanent and induced ones) of the solvent is essential. In Paper I, we formulated a novel integral equation theory to calculate the three-dimensional (3D) site densities and the polarization charge densities of the solvent around a solute.[20] In Paper II, a nonequilibrium free energy profile of the charge-transfer reaction was calculated using the sp-3D-RISM theory.[21] In this paper, we extend our sp-3D-RISM theory to dynamics, which plays an important role in understanding charge-transfer reactions.

As is the case for the conventional RISM theory,[22] our sp-3D-RISM theory can be formulated based on the density functional theory.[20] The free energy functional of the 3D-RISM theory, which is a functional of the site density field, is extended to the functional of both the site density and the site polarization charge in the sp-3D-RISM theory. Both the site density and the site polarization charge are then determined simultaneously to minimize the free energy functional.

TDDFT describes the current of the site density in terms of the functional derivative of the free energy functional. Therefore, given the free energy functional of the equilibrium system, the extension to dynamics can be performed in a relatively easy way through the formulation of TDDFT. An important point to be noted is the difference in the time scales of the site density and the polarization charge. The site density of the solvent relaxes slowly upon a change in the external potential, whereas the response of the electronic polarization is instantaneous. In our present theory, therefore, the polarization charge is determined at each time to minimize the free energy functional associated with a given transient site density, whereas the current of the site density is related to the functional derivative of the free energy functional, as performed in ordinary TDDFT.

Besides addressing the electronic polarization, this study describes—to the best of our knowledge—the first numerical calculation of TDDFT for molecular liquids based on the interaction-site model proposed by Yoshimori.[19] Although Kasahara and Sato performed numerical calculations of the 3D diffusive dynamics of a lithium ion around a solute,[23] their work was limited to the dynamics of a monoatomic molecule in the limit of infinite dilution. They also described the diffusive dynamics of diatomic molecular liquids from the viewpoint of diffusion-controlled reactions, which was, however, limited to the linearized dynamics.[24]

This paper consists of five sections. Section II describes the combination of TDDFT with sp-3D-RISM theory. Computational methods and the systems under consideration are presented in Sec. III. The numerical results for solvation dynamics of charge-transfer reaction systems are presented and the results are briefly discussed in Sec. IV. Finally, we present our concluding remarks in Sec. V.

II. THEORY

A. System under consideration

The system that we consider is a solution of infinite dilution, composed of polyatomic molecules. The solute is spatially fixed. It

is regarded as an external potential on solvent molecules. The solvent molecules are assumed to be rigid. The intermolecular interactions, both solute–solvent and solvent–solvent ones, are described as the sum of the site–site interaction potentials. The solute–solvent and solvent–solvent site–site potentials are isotropic and pairwise additive. In particular, the potential of the solute on a solvent site v is composed of short-range Lennard-Jones (LJ) and electrostatic interactions as

$$u_v(\boldsymbol{r}) = u_v^{\mathrm{LJ}}(\boldsymbol{r}) + Q_v V_{\mathrm{solu}}(\boldsymbol{r}), \tag{1}$$

where Q_v and $V_{\mathrm{solu}}(\boldsymbol{r})$ stand for the partial charge on the solvent site and the electrostatic potential due to the charge distribution of the solute, respectively.

In the sp-3D-RISM theory, the electronic polarization of the solvent is described by means of the charge-response kernel (CRK).[25,26] In the CRK model, Q_v responds linearly to the electrostatic potentials on sites within the same molecule, $V_{v'}$, as

$$Q_v = Q_v^{\mathrm{vac}} + \sum_{v'} K_{vv'} V_{v'}, \tag{2}$$

where the matrix $K_{vv'}$ is referred to as CRK and Q_v^{vac} stands for the partial charge of the isolated molecule.

The average partial charge in the bulk solvent, Q_v^0, deviates from Q_v^{vac} due to solvent–solvent electrostatic interactions. In addition, the average partial charge around the solute is position dependent, denoted as $Q_v(\boldsymbol{r})$, and its deviation from Q_v^0 defines $\delta\Delta Q_v(\boldsymbol{r})$ as

$$Q_v(\boldsymbol{r}) \equiv Q_v^0 + \delta\Delta Q_v(\boldsymbol{r}). \tag{3}$$

The sp-3D-RISM theory describes the equilibrium solvation structure of the solute in terms of $\delta\Delta Q_v(\boldsymbol{r})$ and the distribution function of the solvent site $g_v(\boldsymbol{r})$.

The problem we consider is the response of the solvent to the instantaneous electronic excitation of the solute from the ground (g) to the excited (e) states. The intramolecular geometry of the solute is assumed to be independent of the electronic state, and $u_v^{\mathrm{LJ}}(\boldsymbol{r})$ does not change upon the electronic transition of the solute. On the other hand, $V_{\mathrm{solu}}(\boldsymbol{r})$ of the ground and the excited states, denoted as $V_{\mathrm{solu}}^{\mathrm{g}}(\boldsymbol{r})$ and $V_{\mathrm{solu}}^{\mathrm{e}}(\boldsymbol{r})$, respectively, differ. In the dynamic fluorescence Stokes shift measurement, which is a representative experiment of solvation dynamics, the time development of the transition energy from the excited state to the ground state after the excitation at time $t = 0$ is examined.

The transient distribution function of the solvent site, denoted as $g_v(\boldsymbol{r}, t)$, is equal to the equilibrium distribution in the ground state, $g_v^{\mathrm{g,eq}}(\boldsymbol{r})$, just after the electronic excitation, and it relaxes to the equilibrium distribution in the excited state, $g_v^{\mathrm{e,eq}}(\boldsymbol{r})$. The transient polarization charge on the excited state, denoted as $\delta\Delta Q_v^{\mathrm{e}}(\boldsymbol{r}, t)$, also changes with time, reflecting the relaxation of the solvation structure.

Since the electronic polarization of the solvent responds instantaneously to the change in the electrostatic potential, the initial value of $\delta\Delta Q_v^{\mathrm{e}}(\boldsymbol{r}, t)$ is different from the equilibrium polarization charge in the ground state, $\delta\Delta Q_v^{\mathrm{g,eq}}(\boldsymbol{r})$.

The transient transition energy from the excited state to the ground state is the difference between the total energies of the system before and after the virtual electronic transition to the ground state. Since the electronic polarization of solvent follows the virtual electronic transition immediately, the polarization charge after the transition, $\delta\Delta Q_v^{\mathrm{g}}(\boldsymbol{r}, t)$, is different from $\delta\Delta Q_v^{\mathrm{e}}(\boldsymbol{r}, t)$. Therefore, the change in the total energy includes that of the intramolecular electronic energy of the solvent and the solvent–solvent electrostatic interaction, in addition to the intramolecular electronic energy of the solute and the solute–solvent interaction energy. Considering that the electronic polarization of the solvent is linear to the electrostatic potential and that the solvent–solvent electrostatic interaction is, at most, quadratic to the polarization charge density, the transient transition energy, $\Delta E(t)$, is given as follows:[21]

$$\begin{aligned}\Delta E(t) = \Delta E_{\mathrm{vac}} &+ \int d\boldsymbol{r}\left[V_{\mathrm{solu}}^{\mathrm{g}}(\boldsymbol{r}) - V_{\mathrm{solu}}^{\mathrm{e}}(\boldsymbol{r})\right]\left[Q_v^0 + \delta\Delta Q_v^{\mathrm{e}}(\boldsymbol{r})\right]g_v^{\mathrm{e}}(\boldsymbol{r}) \\ &+ \frac{1}{2}\int d\boldsymbol{r}\left[V_{\mathrm{solu}}^{\mathrm{g}}(\boldsymbol{r}) - V_{\mathrm{solu}}^{\mathrm{e}}(\boldsymbol{r})\right]\left[\delta\Delta Q_v^{\mathrm{g}}(\boldsymbol{r}) - \delta\Delta Q_v^{\mathrm{e}}(\boldsymbol{r})\right]g_v^{\mathrm{e}}(\boldsymbol{r}).\end{aligned} \tag{4}$$

Here, the first term stands for the electronic transition energy in a vacuum, the second term means the change in the solute–solvent electrostatic interaction energy if the polarization charge density is fixed on the virtual transition, and the last term is the energy associated with the relaxation of the polarization charge.

B. Free energy functional of sp-3D-RISM theory

The free energy of the system is given as a functional of $g_v(\boldsymbol{r})$ and $\delta\Delta Q_v(\boldsymbol{r})$ as follows:[20]

$$\begin{aligned}\mathcal{F}\left[\{g_v(\boldsymbol{r}), \delta\Delta Q_v(\boldsymbol{r})\}\right] = \Omega_0\left[\{g_v(\boldsymbol{r})\}\right] + \Omega_{\mathrm{pol}}\left[\{g_v(\boldsymbol{r}), \delta\Delta Q_v(\boldsymbol{r})\}\right] \\ + \sum_v \rho_v \int d\boldsymbol{r} g_v(\boldsymbol{r}) u_v^{\mathrm{LJ}}(\boldsymbol{r}) + \sum_v \rho_v \int d\boldsymbol{r} g_v(\boldsymbol{r}) \\ \times \left[Q_v^0 + \delta\Delta Q_v(\boldsymbol{r})\right] V_{\mathrm{solu}}(\boldsymbol{r}),\end{aligned} \tag{5}$$

where ρ_v denotes the number density of the site v. The first term of the right-hand side of Eq. (5) is the conventional free energy functional of the 3D-RISM theory, which depends on the choice of closure. The functional for the hypernetted-chain (HNC) closure is given by

$$\begin{aligned}\Omega_0\left[\{g_v(\boldsymbol{r})\}\right] = k_B T \sum_v \rho_v \int d\boldsymbol{r}\Big[g_v(\boldsymbol{r}) \ln g_v(\boldsymbol{r}) - \frac{1}{2}\{h_v(\boldsymbol{r})\}^2 \\ - h_v(\boldsymbol{r}) + \frac{1}{2} h_v(\boldsymbol{r}) c_v(\boldsymbol{r})\Big],\end{aligned} \tag{6}$$

where k_B and T denote the Boltzmann constant and the absolute temperature, respectively. The definitions of the total correlation function, $h_v(\boldsymbol{r})$, and the direct correlation function, $c_v(\boldsymbol{r})$, follow those of the ordinary 3D-RISM theory. The functional for the Kovalenko–Hirata (KH) closure is given by

$$\begin{aligned}\Omega_0\left[\{g_v(\boldsymbol{r})\}\right] = k_B T \sum_v \rho_v \int d\boldsymbol{r}\Big[\Theta(-h_v(\boldsymbol{r}))\Big\{g_v(\boldsymbol{r}) \ln g_v(\boldsymbol{r}) \\ - \frac{1}{2}\{h_v(\boldsymbol{r})\}^2 - h_v(\boldsymbol{r})\Big\} + \frac{1}{2} h_v(\boldsymbol{r}) c_v(\boldsymbol{r})\Big],\end{aligned} \tag{7}$$

where $\Theta(x)$ is the Heaviside step function, which is unity at $x > 0$ and zero at $x < 0$.

The second term of Eq. (5) is given by

$$\begin{aligned}\Omega_{\rm pol}[\{g_v(\boldsymbol{r}),\delta\Delta Q_v(\boldsymbol{r})\}] &= \sum_{vv'}\iint \rho_v h_v(\boldsymbol{r}) Q_v^0 W(\boldsymbol{r},\boldsymbol{r}')\rho_{v'} g_{v'}(\boldsymbol{r}')\delta\Delta Q_{v'}(\boldsymbol{r}')d\boldsymbol{r}d\boldsymbol{r}' \\ &+\frac{1}{2}\sum_{vv'}\iint \rho_v g_v(\boldsymbol{r})\delta\Delta Q_v(\boldsymbol{r}) W(\boldsymbol{r},\boldsymbol{r}')\rho_{v'} g_{v'}(\boldsymbol{r}')\delta\Delta Q_{v'}(\boldsymbol{r}')d\boldsymbol{r}d\boldsymbol{r}' \\ &-\frac{1}{2}\sum_{vv'}\iint \rho_v g_v(\boldsymbol{r})\delta\Delta Q_v(\boldsymbol{r}) M_{vv'}^{-1}(\boldsymbol{r},\boldsymbol{r}') \\ &\times \rho_{v'} g_{v'}(\boldsymbol{r}')\delta\Delta Q_{v'}(\boldsymbol{r}')d\boldsymbol{r}d\boldsymbol{r}', \end{aligned} \tag{8}$$

where

$$W(\boldsymbol{r},\boldsymbol{r}') = \frac{\mathrm{erf}(\alpha|\boldsymbol{r}-\boldsymbol{r}'|)}{|\boldsymbol{r}-\boldsymbol{r}'|}, \tag{9}$$

$$M_{vv'}(\boldsymbol{r},\boldsymbol{r}') = K_{vv'}\langle\rho_v(\boldsymbol{r})\rho_{v'}(\boldsymbol{r}')\rangle_{\rm s}. \tag{10}$$

The first term of the right-hand side of Eq. (8) stands for the electrostatic interaction between the average and polarization charges of the solvent molecules, and the second term does likewise between polarization charges. The last term corresponds to the intramolecular electronic energy of the solvent associated with the distortion of the electronic distribution. The screening factor in Eq. (9), $\mathrm{erf}(\alpha|\boldsymbol{r}-\boldsymbol{r}'|)$, is introduced to exclude the self-interaction. The subscript "s" of the angular bracket in Eq. (10) means that only the correlation within the same molecule is taken into account.

The third and the fourth terms of the right-hand side of Eq. (5) correspond to the LJ and the electrostatic interactions between the solute and the solvent, respectively.

C. TDDFT coupled with sp-3D-RISM theory

The TDDFT for molecular liquids based on the interaction-site model was first formulated by Yoshimori for a nonpolarizable solvent.[19] In his theory, the time development of the site density follows the conservation law as

$$\rho_v\frac{\partial g_v(\boldsymbol{r},t)}{\partial t} = -\nabla\cdot\boldsymbol{j}_v(\boldsymbol{r},t), \tag{11}$$

and the current density of the site v, denoted as $\boldsymbol{j}_v(\boldsymbol{r},t)$, is related to the functional derivative of the free energy functional as

$$\boldsymbol{j}_v(\boldsymbol{r},t) = -\sum_{v'}\int d\boldsymbol{r}'\frac{\boldsymbol{D}_{vv'}(\boldsymbol{r},\boldsymbol{r}')}{\rho_{v'}k_{\rm B}T}\cdot\nabla'\frac{\delta F[\{g_v(\boldsymbol{r},t)\}]}{\delta g_{v'}(\boldsymbol{r}')}. \tag{12}$$

The kernel function, $\boldsymbol{D}_{vv'}(\boldsymbol{r},\boldsymbol{r}')$, is a tensor that is given by the time integral of the time correlation function of random site currents. Hereafter, we refer to $\boldsymbol{D}_{vv'}(\boldsymbol{r},\boldsymbol{r}')$ as the "diffusion kernel."

In the solvent-polarizable case, the solvation structure around the solute is characterized by the sets of the site distribution functions, $\{g_v(\boldsymbol{r})\}$, and the site polarization charges, $\{\delta\Delta Q_v(\boldsymbol{r})\}$. Therefore, the extension of Yoshimori's theory should provide the time development of both functions.

Since the response of the electronic polarization of the solvent is much faster than the nuclear motion of the solvent, it is considered to always keep its stable state for a given nuclear configuration of the solvent. Therefore, we require that $\{\delta\Delta Q_v(\boldsymbol{r},t)\}$ minimizes $\mathcal{F}[\{g_v(\boldsymbol{r},t),\delta\Delta Q_v(\boldsymbol{r},t)\}]$ at any time for $\{g_v(\boldsymbol{r},t)\}$, given as

$$\left.\frac{\delta\mathcal{F}[\{g_v(\boldsymbol{r},t),\delta\Delta Q_v(\boldsymbol{r},t)\}]}{\delta\delta\Delta Q_v(\boldsymbol{r},t)}\right|_{g_v(\boldsymbol{r},t)} = 0, \tag{13}$$

which is equivalent to the equation that determines $\{\delta\Delta Q_v(\boldsymbol{r})\}$ in the sp-3D-RISM theory.

The conservation law, Eq. (11), must hold irrespective of the electronic polarizability of the solvent. Equation (12) is also employed in the solvent-polarizable case as

$$\boldsymbol{j}_v(\boldsymbol{r},t) = -\sum_{v'}\int d\boldsymbol{r}'\frac{\boldsymbol{D}_{vv'}(\boldsymbol{r},\boldsymbol{r}')}{\rho_{v'}k_{\rm B}T}\nabla'\frac{\delta F[\{g_v(\boldsymbol{r},t),\delta\Delta Q_v(\boldsymbol{r},t)\}]}{\delta g_{v'}(\boldsymbol{r}',t)}. \tag{14}$$

In the calculation of the functional derivative in Eq. (14), although $\{\delta\Delta Q_v(\boldsymbol{r})\}$ changes with $\{g_v(\boldsymbol{r},t)\}$, in principle, $\{\delta\Delta Q_v(\boldsymbol{r})\}$ can be kept constant as long as Eq. (13) holds.

The substitution of Eq. (5) gives the functional derivative in Eq. (14) as

$$\left.\frac{\delta F[\{g_v(\boldsymbol{r},t),\delta\Delta Q_v(\boldsymbol{r},t)\}]}{\rho_v\delta g_v(\boldsymbol{r},t)}\right|_{\delta\Delta Q_v(\boldsymbol{r},t)} = u_v^{\rm CRK}(\boldsymbol{r},t) + \frac{\delta\Omega_0[\{g_v(\boldsymbol{r},t)\}]}{\rho_v\delta g_v(\boldsymbol{r},t)}, \tag{15}$$

where $u_v^{\rm CRK}(\boldsymbol{r},t)$ corresponds to the renormalized potential in the sp-3D-RISM theory, defined as

$$\begin{aligned}u_v^{\rm CRK}(\boldsymbol{r},t) &= u_v^{\rm LJ}(r) + Q_v^0 V_{\rm solu}(r) \\ &+ \left.\frac{\delta\Omega_{\rm pol}[\{g_v(\boldsymbol{r},t),\delta\Delta Q_v(\boldsymbol{r},t)\}]}{\rho_v\delta g_v(\boldsymbol{r},t)}\right|_{\delta\Delta Q_v(\boldsymbol{r},t)}. \end{aligned} \tag{16}$$

Furthermore, substitution of Eq. (6) into Eq. (15) yields

$$\left.\frac{\delta F[\{g_v(\boldsymbol{r},t),\delta\Delta Q_v(\boldsymbol{r},t)\}]}{\rho_v\delta g_v(\boldsymbol{r},t)}\right|_{\delta\Delta Q_v(\boldsymbol{r},t)} = u_v^{\rm eff}(\boldsymbol{r},t) + k_{\rm B}T\ln g_v(\boldsymbol{r},t), \tag{17}$$

where the effective potential for the HNC case is given by

$$u_v^{\rm eff,HNC}(\boldsymbol{r},t) = u_v^{\rm CRK}(\boldsymbol{r},t) + k_{\rm B}T[c_v(\boldsymbol{r},t) - h_v(\boldsymbol{r},t)]. \tag{18}$$

The effective potential for the KH case can also be derived in a similar way as

$$u_v^{\mathrm{eff,KH}}(\boldsymbol{r},t)=\begin{cases} u_v^{\mathrm{CRK}}(\boldsymbol{r},t)+k_{\mathrm{B}}T[c_v(\boldsymbol{r},t)-h_v(\boldsymbol{r},t)], & h_v<0 \\ u_v^{\mathrm{CRK}}(\boldsymbol{r},t)+k_{\mathrm{B}}T[c_v(\boldsymbol{r},t)-\ln g_v(\boldsymbol{r},t)], & h_v\geq 0. \end{cases} \tag{19}$$

It should be stressed here that although the expressions of the effective potential are given only for the HNC and the KH closures, the theoretical formulation of our TDDFT is not limited to these two closures. Given a closed analytical expression of the free energy functional, we can derive the expression of the effective potential for the corresponding closure in a similar way through the functional derivative.

D. Local and diagonal approximation of diffusion kernel

The diffusion kernel in Eqs. (12) and (14), $\boldsymbol{D}_{vv'}(\boldsymbol{r},\boldsymbol{r}')$, is nonlocal, in principle, that is, the driving force at position $\boldsymbol{r}'$ induces diffusive current at a different position $\boldsymbol{r}$. In addition, the diffusion kernel can possess a nonzero off-diagonal component, which means that the driving force on a site v' results in the current of a different site v and that the driving force in one direction exerts the site current in another direction. The derivation of such a diffusion kernel is quite difficult, and its numerical treatment is almost impossible. Therefore, some kind of approximation for the diffusion kernel must be introduced to make our TDDFT numerically tractable.

In this work, we employ a simple approximation as

$$\boldsymbol{D}_{vv'}(\boldsymbol{r},\boldsymbol{r}';t)=\rho_v D_{\mathrm{T},v} g_v(\boldsymbol{r},t)\delta_{vv'}\delta(\boldsymbol{r}-\boldsymbol{r}')\mathbf{1}, \tag{20}$$

where $\mathbf{1}$ stands for the unit tensor and $D_{\mathrm{T},v}$ denotes the translational diffusion coefficient of a molecule to which the site v belongs. Equation (20) is equivalent to the approximation introduced by Kasahara and Sato for the Smoluchowski equation for a diatomic molecular liquid.[24] This approximation becomes exact when applied to the diffusive motion of monoatomic solutes of infinite dilution.

The substitution of Eqs. (17) and (20) into Eq. (14) gives

$$\boldsymbol{j}_v(\boldsymbol{r},t)=-\rho_v D_{\mathrm{T},v}\left[\nabla g_v(\boldsymbol{r},t)+\frac{g_v(\boldsymbol{r},t)}{k_{\mathrm{B}}T}\nabla u_v^{\mathrm{eff}}(\boldsymbol{r},t)\right]. \tag{21}$$

Equation (21) coupled with Eq. (11) reduces to a simple diffusion equation under the time-dependent effective potential, $u_v^{\mathrm{eff}}(\boldsymbol{r},t)$. In addition, Eqs. (11) and (21) reduce to the site–site Smoluchowski–Vlasov (SSSV) equation[27] when they are applied to the linear fluctuation of the nonpolarizable solvent in the absence of an external potential, although, for brevity, the proof is not included here.

Considering that all the dynamics of one-component liquid is scaled by a single parameter, D_{T}, in this approximation, one may consider that this approximation can only describe the translational dynamics of the solvent, and the information on the rotational motion is lost. As was discussed in detail on the dynamics of bulk water,[28] however, the reorientation of a molecule is described in the interaction-site model as the correlated translational diffusion of intramolecular sites, and our TDDFT with the local and diagonal approximation of the diffusion kernel can also capture the reorientation of solvent in the same way. On the other hand, the Markovian approximation in the time domain neglects the slow friction on both translational and reorientational modes, which is questionable for the reorientation of liquid water.[29] The inclusion of the slow memory is one of our future plans as will be discussed in Sec. IV F.

III. COMPUTATIONAL DETAILS

The theory formulated in this study is applied to two model systems. Both systems are aqueous solutions of infinite dilution under ambient conditions, and the electronic polarizability of solvent water is described by the CRK model. The CRK of water is an input parameter in our sp-3D-RISM theory, which was taken from the literature.[26] The temperature and the number density of the solvent water are 298.0 K and 0.033 34 Å^{-3}, respectively, and the self-diffusion coefficient of water, 2.3 × 10^{-9} m^2/s, is taken from an experiment under ambient conditions.[30] The solute of the first model system is a sodium (Na) atom, whose charge changes from 0 to +e upon the instantaneous transition from the ground to the excited states. The second solute is *p*-nitroaniline (pNA), which experiences intramolecular charge transfer upon the electronic transition. pNA is a push–pull type of aromatic dye and has been used as a solvatochromic probe. It has also been employed as a probe molecule of intramolecular charge-transfer reactions and solvation dynamics.[31–33] Using sp-3D-RISM theory, the nonequilibrium free energy profiles of these systems were investigated in our previous study and detailed parameters are summarized there.[21] In both systems, the energy difference between the two states in a vacuum, denoted as ΔE_{vac}, is set to be zero, for simplicity.

The initial solvation structure, that is, the equilibrium solvation structure in the ground state, was calculated using sp-3D-RISM theory.[20] The final state, the equilibrium solvation structure in the excited state, was also calculated in the same way for comparison with TDDFT calculation. In the sp-3D-RISM theory, the partial structure factors of the neat solvent, together with the average partial charge of the bulk solvent, Q_v^0, have to be determined prior to the calculation on solute–solvent systems. The calculation on neat solvent water was performed using the solvent-polarizable reference interaction-site model (sp-RISM) theory proposed by Naka and co-workers.[34] The dielectrically consistent RISM (DRISM) correction was introduced there to adjust the static dielectric constant to be 78.5.[35,36] In the calculation of the neat solvent, the radial coordinate was discretized with a grid size of 0.01 Å and a grid number of 16 384. The calculations on the equilibrium solvation structures of solute–solvent systems were performed on 3D cubic grids. The number of grids is 128^3 for both systems, and the grid sizes are 0.5 Å for Na and 0.25 Å for pNA. The value of α in Eq. (9) was set to be 0.5 Å^{-1}, as in our previous studies.[20,21]

The TDDFT calculation was performed on the same spatial grid as the sp-3D-RISM calculation, with a time grid of Δt = 1 fs. The boundary condition at the surfaces of the cell is given by

$$\forall v, t, \quad g_v(\boldsymbol{r}, t) \equiv 1, \tag{22}$$

allowing the site current into/out of the cell. The time propagation was performed using a partially implicit algorithm in which $g_v(\boldsymbol{r}, t)$ and $u_v^{\mathrm{eff}}(\boldsymbol{r}, t)$ on the right-hand side of Eq. (21) were evaluated at time $t + \Delta t$ and t, respectively, for the time propagation from t to $t + \Delta t$. The 3D diffusion was replaced with the alternation of 1D diffusions by means of the alternating direction implicit (ADI) algorithm.[23] The details of the time-propagation algorithm are summarized in the supplementary material.

All calculations were conducted using the RISM integrated calculator (RISMiCal) program package developed by us.[37]

IV. RESULTS AND DISCUSSION

A. Time-dependent response of transition energy

Figure 1 shows the time dependence of the transition energy from the excited state to the ground state after the excitation at $t = 0$, which corresponds to the dynamic Stokes shift in the transient fluorescence spectroscopy. The results of the Na atom and pNA in water are plotted in Figs. 1(a) and 1(b), respectively. The transition energy increases with increasing time, reflecting the energetic stabilization in the excited state. The equilibrium solvation structure in the excited state was calculated separately using sp-3D-RISM theory. The equilibrium value of the transition energy is also shown in Fig. 1 (dashed lines), for comparison. The transition energy almost converges to the equilibrium value within 2 ps in both systems.

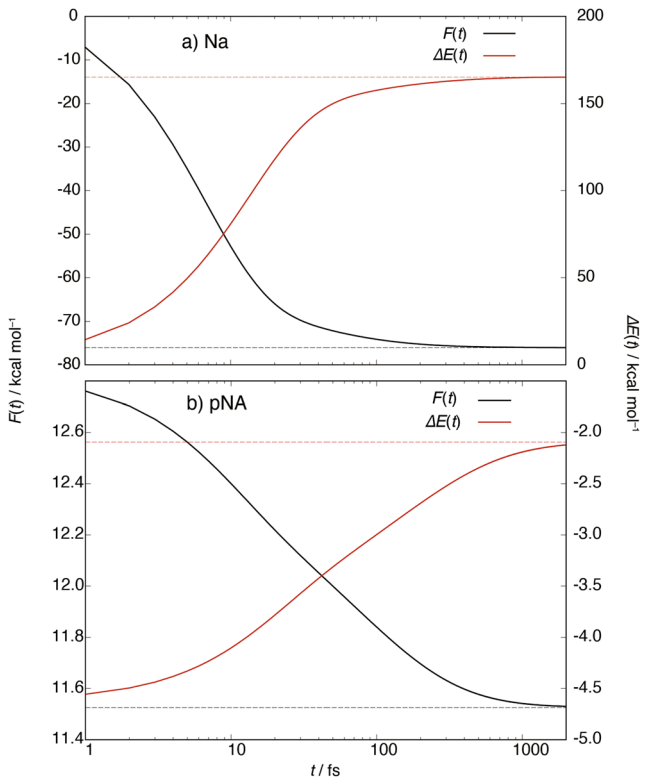

FIG. 1. Time dependence of the transition energy, $\Delta E(t)$ (red, right axis), and the free energy, $\mathcal{F}(t)$ (black, left axis), of the (a) Na atom and (b) pNA in water after excitation from the ground state to the excited state at $t = 0$. The horizontal dashed lines indicate the corresponding equilibrium values at $t = \infty$ of $\Delta E(t)$ (red) and $\mathcal{F}(t)$ (black).

The relaxation of the transition energy is bimodal in both systems. The faster relaxation occurs in the time scale of several tens of femtoseconds, whereas the time scale of the slower mode is several hundreds of femtoseconds. The bimodal relaxation is often observed experimentally in solvation dynamics in solution.[1,7] The theoretical calculation carried out by Nishiyama and co-workers, using the surrogate and the SSSV theories, also reported the bimodal relaxation.[38] Comparing the solvation dynamics of the two systems, the relative amplitude of the slower mode of pNA is larger than that of the Na atom. Nishiyama and co-workers reported that the relative amplitude of the slower mode increases with increasing multipolar character of the electronic transition of the solute. Our present result is consistent with their result.

Since our theory obtains the transient site distribution functions, $g_v(\boldsymbol{r}, t)$, and the transient site polarization charges, $\delta\Delta Q_v(\boldsymbol{r}, t)$, at each time, we can calculate the transient free energy at the time $\mathcal{F}(t)$ by substituting $g_v(\boldsymbol{r}, t)$ and $\delta\Delta Q_v(\boldsymbol{r}, t)$ into the free energy functional, Eq. (5). The calculation of the transient free energy during solvation dynamics is almost impossible by MD simulation, and the calculation of $\mathcal{F}(t)$ is one of the advantages of the TDDFT-based theories over MD simulation.

The transient free energies of both systems are also plotted in Fig. 1. The free energy decreases with time, as expected, and the values of $\mathcal{F}(t)$ at the longest time of our calculation (2 ps) are close to those calculated by the equilibrium sp-3D-RISM theory. The trend of the relaxation of $\mathcal{F}(t)$ follows that of $\Delta E(t)$. The relaxation is bimodal, consisting of relaxation modes of several tens of femtoseconds and several hundreds of femtoseconds, and the relative amplitude of the slower mode of pNA is larger than that of the Na atom. The relationship between the relaxation dynamics of $\mathcal{F}(t)$ and $\Delta E(t)$ will be discussed in Sec. IV E.

B. Dynamics of solvation structure and polarization charge density

The time developments of $g_v(\boldsymbol{r}, t)$ and $\delta\Delta Q_v(\boldsymbol{r}, t)$ of both systems are reported in this subsection. First, we examine the results of the simpler system, the Na atom in water.

Figure 2 shows the time development of the site distribution functions around the Na atom. The distribution functions just before the excitation, $t = -0$ fs, and the final equilibrium state, $t = \infty$, were calculated using the equilibrium sp-3D-RISM. Since the nuclear motion of the solvent cannot follow the electronic transition of the solute immediately, the distribution functions just after the excitation, $t = +0$ fs, are equal to those at $t = -0$ fs. Before the transition, the solvation structure is not strong, and the orientation of the solvent around the solute is almost random because there is no electrostatic interaction between the solute and the solvent. In the equilibrium state of the excited state, the first peak of $g_O(\boldsymbol{r}, t)$ is strengthened and shifted to shorter distance, reflecting

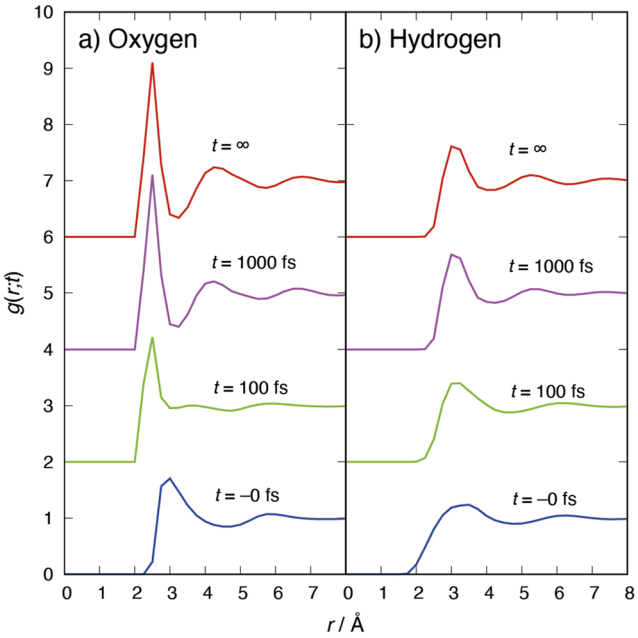

FIG. 2. Transient site distribution functions of (a) O-atom and (b) H-atom of water around the model Na atom. The functions at $t = -0$ fs and $t = \infty$ were calculated by equilibrium sp-3D-RISM theory, and those at $t = 100$ fs and 1000 fs were obtained from the dynamics calculation. The values of t are indicated within the panels, and the functions other than those at $t = -0$ fs are vertically shifted.

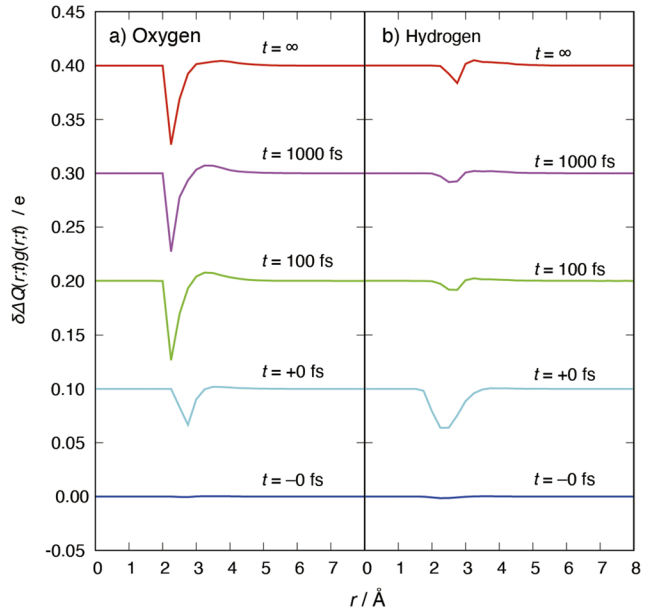

FIG. 3. Transient site polarization charge densities, $\delta\Delta Q_v(\boldsymbol{r}, t)g_v(\boldsymbol{r}, t)$, of the (a) O-atom and (b) H-atom of water around the model Na atom. The values of t are indicated within the panels. The functions at $t = -0$ fs, +0 fs, and $t = \infty$ were found using equilibrium sp-3D-RISM calculation, and those at $t = 100$ fs and 1000 fs were obtained from the dynamics calculation. The functions other than those at $t = -0$ fs are vertically shifted.

the strong attractive interaction between Na^+ and the negatively charged O-atom of water. The first peak of $g_H(\boldsymbol{r}, t = \infty)$ lies at longer distance than that of $g_O(\boldsymbol{r}, t = \infty)$, which describes that the H-atom of water in the first solvation shell orients to an outer direction.

The relaxation of the solvation structure proceeds from the equilibrium solvation of the neutral ground state to that of the charged excited state. The transient solvation structures at $t = 100$ fs and 1000 fs are shown in Fig. 2. At $t = 100$ fs, the positions of the first peak are close to the final state, whereas the second peaks at the initial state remain at almost the same positions. Therefore, the dynamics up to 100 fs corresponds to the reorganization of the first solvation shell. At $t = 1000$ fs, the solvation structure at longer distance is also relaxed, and the qualitative features of $g_v(\boldsymbol{r}, t)$ resemble those of the final equilibrium state.

The site polarization charge densities around the Na atom at various times, $\delta\Delta Q_v(\boldsymbol{r}, t)g_v(\boldsymbol{r}, t)$, are shown in Fig. 3. The electronic polarization around the neutral Na atom, $t = -0$ fs, is marginal, whereas the solvent experiences strong electronic polarization in the equilibrium solvation state, $t = \infty$, as expected. Since the electronic polarization of the solvent can respond to the electronic transition of the solute immediately, strong polarization is observed in the first solvation shell just after the electronic transition of the solute, $t = +0$ fs.

The nuclear distribution of the solvent at $t = +0$ fs is fixed to that at $t = -0$ fs. The orientation of water in the first solvation shell is relatively random, and some water molecules orient their H-atoms toward the solute. When the solute Na atom is suddenly charged to $+e$, with keeping the orientation of the solvating water, the H-atom in contact with the Na atom experiences strong negative polarization, which explains the strong negative peak of $\delta\Delta Q_H(\boldsymbol{r}, t)g_H(\boldsymbol{r}, t)$ at $t = +0$ fs and $r = 2.2$ Å, as shown in Fig. 3(b). After the reorientational relaxation of water in the first solvation shell, $t = 100$ fs, the negative polarization on the H-atom is reduced, whereas the negative polarization on the O-atom is strengthened, as shown in Fig. 3(a). The positions of the peaks of the polarization charge density also shift following the peak shift of the site distribution function, $g_v(\boldsymbol{r}, t)$, as shown in Fig. 2. The changes in the polarization charge densities after 100 fs appear small in Fig. 3. This is because the electronic polarization is limited to almost within the first solvation shell. Although the reorganization of the long-range structure occurs after 100 fs (as shown in Fig. 2), it is hardly reflected in the polarization charge density because little electronic polarization exists there.

The relaxation of the site distribution around the pNA solute is shown in Fig. 4. Only the in-plane contour plots are shown there, for simplicity. The difference in the equilibrium solvation structures of the ground and the excited states, $t = -0$ fs and ∞, respectively, is relatively small because the change in the partial charges of the solute is not large. A remarkable difference is found in $g_H(\boldsymbol{r}, t)$ around the nitro group. Weak distribution of the H-atom around the nitro oxygen is found at $t = -0$ fs [Fig. 4(e)], whereas it disappears at

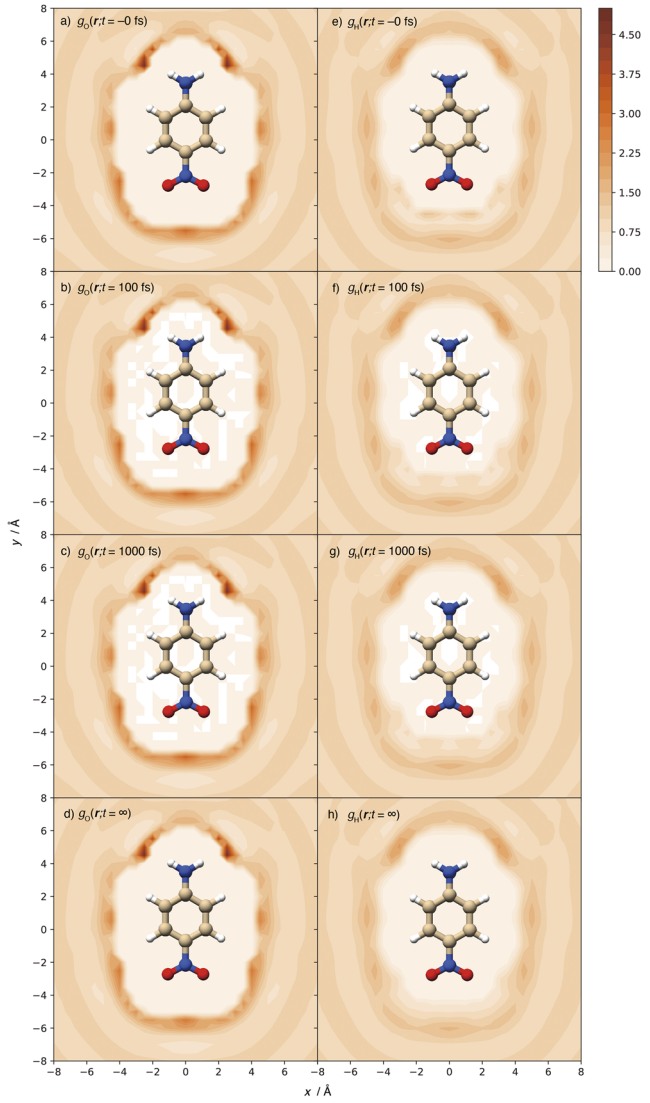

FIG. 4. In-plane contour plot of the site distribution function around pNA, $g_v(\boldsymbol{r}, t)$. Distributions of the O-atom are shown in panels (a)–(d) and those of the H-atom are shown in panels (e)–(h). The values of t are +0 fs [(a) and (e)], 100 fs [(b) and (f)], 1000 fs [(c) and (g)], and ∞ [(d) and (h)].

$t = \infty$ [Fig. 4(h)]. The distribution of the H-atom is interpreted as the hydrogen bond between the H-atom of the solvent water and the nitro oxygen of the solute pNA, and the change in the strength of the hydrogen bond is ascribed to the decrease in the negative partial charge on the nitro oxygen.

The distribution of the H-atom around the nitro oxygen decreases with time, as seen in Figs. 4(f) and 4(g). Upon comparing $g_H(\boldsymbol{r}, t)$ at 1000 fs with that at $t = \infty$, it is evident that the distribution associated with the hydrogen bond is stronger in the former, which may be related to the slower component of the solvation dynamics [see Fig. 1(b)]. Although the corresponding relaxation dynamics of the O-atom is present, it is difficult to recognize in Figs. 4(a)–4(d) because the magnitude of the change is weak. The detailed structural relaxation around pNA will be discussed in Sec. IV D in terms of $g_v(\boldsymbol{r}, t) - g_v(\boldsymbol{r}, t = \infty)$.

The site polarization charge densities around pNA at various times are plotted in Fig. 5. The in-plane contour plots are exhibited there, as is the case of the site distribution functions in Fig. 4. The strong negative polarization of the O-atom is found around the amino group in Figs. 5(a)–5(d), whereas the polarization charge density of the H-atom is positive around the nitro group in Figs. 5(e)–5(h). Both polarizations are ascribed to the solute–solvent direct hydrogen bond. The amplitudes of these polarization

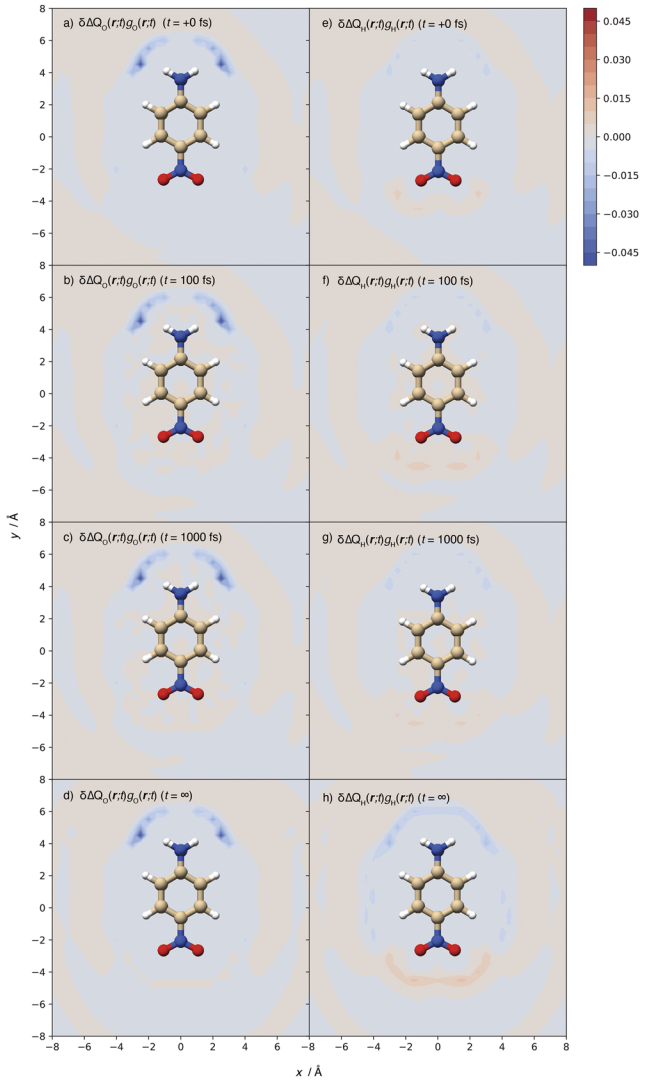

FIG. 5. In-plane contour plot of the site polarization charge density around pNA, $\delta\Delta Q_v(\boldsymbol{r}, t)g_v(\boldsymbol{r}, t)$. Polarization charges on the O-atom are shown in panels (a)–(d) and those on the H-atom are shown in panels (e)–(h). The values of t are +0 fs [(a) and (e)], 100 fs [(b) and (f)], 1000 fs [(c) and (g)], and ∞ [(d) and (h)].

charge densities vary with time, reflecting the time development of the site distribution functions shown in Fig. 4. This demonstrates that our present theory can provide detailed dynamics of the 3D solvation structure, including the electronic polarization of solvent molecules.

C. Comparison with solvation dynamics without electronic polarization of solvent

We now examine how the electronic polarization of the solvent affects the solvation dynamics. The transient transition energy, $\Delta E(t)$, is separated into three terms in Eq. (4). The first term is the transition energy in a vacuum, which is invariant during the solvation dynamics, and assumed to be zero in this study. The second term is the change in the solute–solvent electrostatic interaction under the condition that the polarization charge density does not respond to hypothetical electronic transition at each time, and the third term is ascribed to the relaxation of the electronic polarization of the solvent. In Fig. 6, the contributions of the second and the third terms are plotted separately for the Na atom in water.

Figure 6 demonstrates that the contribution of the second term is dominant. The relaxation of the polarization charge density makes a negative contribution because it stabilizes the state after the virtual transition, and its contribution is hardly dependent on time. These tendencies are also observed for pNA in water, although the results are not shown (for brevity).

We calculated the nonequilibrium free energy profiles of the same systems in our previous study.[21] The division of the free energy profile into the fixed polarization and the polarization relaxation terms was also performed there. The contribution of the latter was small, and almost constant, along the solvation coordinate. Therefore, the constant contribution of the third term is consistent with the nonequilibrium free energy profile in our previous study if we regard the solvation dynamics as the relaxation along the nonequilibrium free energy profile. The validity of this picture will be examined in Sec. IV E.

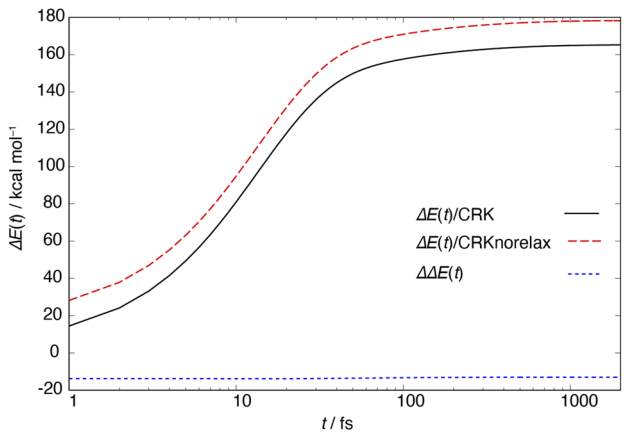

FIG. 6. Transient transition energy of the Na atom in water (CRK), separated into the contributions of the second (CRKnorelax) and the third [$\Delta\Delta E(t)$] terms of Eq. (4).

The numerical calculations of the solvation dynamics of both systems were also performed without including the electronic polarization of the solvent in the calculation of solute–solvent systems in order to examine the effects of the electronic polarization on the solvent dynamics. In these calculations, the partial charges on the solvent sites are determined using sp-RISM theory for the neat solvent, taking the electronic polarization into account.

In both systems, the electronic polarization of the solvent slightly retards the solvation dynamics, as demonstrated in Fig. 7. The retardation effects on $\Delta E(t)$ and $\mathcal{F}(t)$ are similar, and the degree of the retardation is about 10%–20%. The weak retardation of the solvation dynamics by the electronic polarization of the solvent can be explained qualitatively in two different ways. The first is based on the continuum dielectric model.[1,39] In the monopole case as the Na atom in water, dielectric continuum theory predicts that the solvation time is equal to the longitudinal dielectric relaxation time, τ_L, which is related to the dielectric relaxation time, τ_D, as follows:[5]

$$\tau_L = \frac{\epsilon_\infty}{\epsilon_0}\tau_D. \tag{23}$$

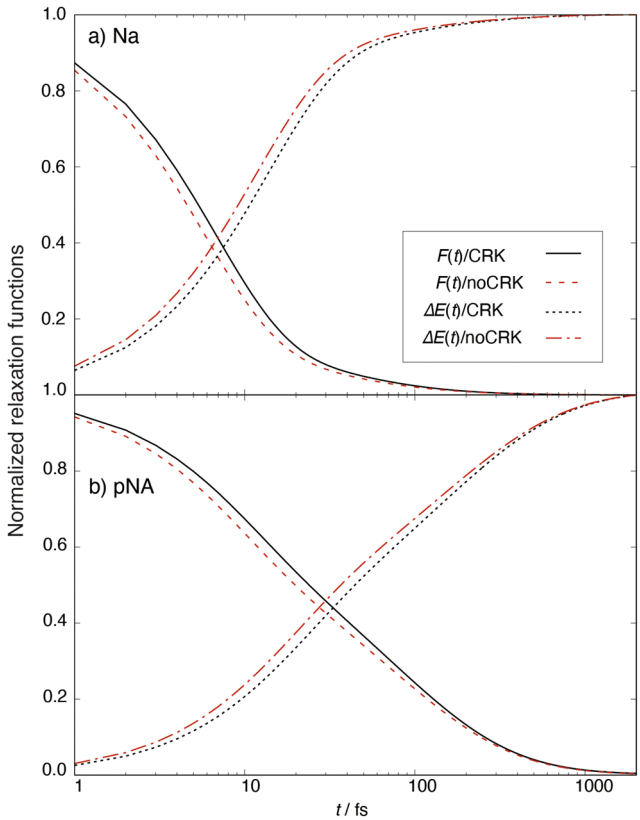

FIG. 7. Transient transition energy, $\Delta E(t)$, and free energy, $\mathcal{F}(t)$, of the (a) Na atom and (b) pNA in water. The dynamics with (black, CRK) and without (red, noCRK) the electronic polarization for the solute–solvent systems are compared. The relaxation functions are normalized to their respective absolute values of the difference between t = +0 and ∞.

The dielectric constants in the high-frequency (optical) and the zero-frequency limits are denoted here as ϵ_∞ and ϵ_0, respectively. Assuming that the dielectric relaxation time, τ_D, is not affected by the electronic polarization, τ_L is increased in an electronically polarizable solvent by ϵ_∞ because $\epsilon_\infty = 1$ in an electronically nonpolarizable system. The value of ϵ_∞, derived in our previous study, is 1.25,[20] which suggests that the electronic polarization retards the solvation dynamics by about 25%.

Another qualitative explanation is the decrease in the curvature of the nonequilibrium free energy profile. We have evaluated the nonequilibrium free energy profiles of the present systems in our previous study as a function of z, the parameter that characterizes hypothetical states between the ground and the excited states.[21] We found that introduction of the electronic polarization of the solvent decreases the curvature of the free energy profile by about 10%–20%. Since the curvature of the free energy profile describes the thermodynamic effective force to restore the solvation structure, the decrease in the curvature is expected to increase the solvation time through the decrease in the restoring force. The two explanations above would have the same physical origin because the curvature of the nonequilibrium free energy profile is related to ϵ_∞ in a dielectric continuum model.

The experimental value of ϵ_∞ of water under ambient conditions is 1.78, and the CRK model and the sp-3D-RISM theory underestimate ϵ_∞ for several reasons.[20] Therefore, based on the idea above that the retardation of the solvation dynamics by the electronic polarization is related to the longitudinal dielectric relaxation time and the curvature of the nonequilibrium free energy profile, the retardation in real systems is expected to be larger than that in the present calculation.

D. Assignments of bimodal relaxation

The assignments of the fast and the slow modes of the solvation dynamics, as shown in Fig. 1, are now discussed. The origin of the larger relative amplitude of the slower mode of pNA compared with that of the Na atom is also analyzed.

The transient site distribution functions around the Na atom are subtracted by the corresponding functions at $t = \infty$ and plotted in Fig. 8. The oscillations of the functions of the O- and H-atoms at $t = 0$ are antiphase to each other, particularly within the first solvation shell, indicating that the orientational mode within the first solvation shell is strongly coupled to the electronic transition of the solute.[27,28,40] After 100 fs, the strong oscillation within the first solvation shell is diminished, whereas the relaxation of the distributions at large distances is not so remarkable. Therefore, the relaxation from $t = 0$ fs to 100 fs is mainly assigned to the reorientation of water within the first solvation shell. At $t = 1000$ fs, on the other hand, oscillations of the remaining distributions of the O-atom and the H-atom are in-phase with each other, and the contribution of the longer distance is strong. The slower mode of the solvation dynamics is thus assigned to the long-range translational diffusion.

Nishiyama and co-workers analyzed the solvation dynamics of multipolar solutes in a polar solvent using surrogate theory coupled with the SSSV theory.[38] Based on the division of the collective intermediate scattering function into the translational and the reorientational modes, they assigned the faster and the slower relaxation

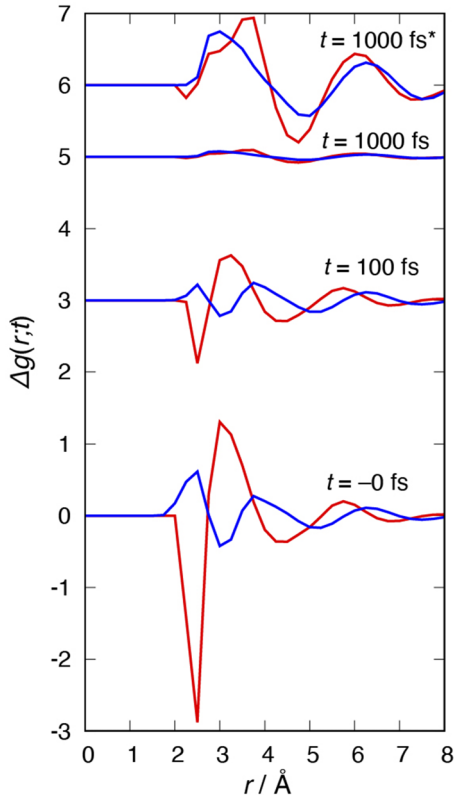

FIG. 8. Difference in the transient site distribution functions around the Na atom from the equilibrium distribution in the excited state, $g_\upsilon(\boldsymbol{r}, t) - g_\upsilon(\boldsymbol{r}, t = \infty)$. The distributions of the O- and H-atoms are plotted with red and blue curves, respectively. The functions at different times are shifted vertically, and the values of t are indicated in the figure. The distribution functions at $t = 1000$ fs have been magnified by multiplying by 10 (top curves).

modes to the reorientation and the translation of the polar solvent, respectively. Our present assignment is thus consistent with that of Nishiyama and co-workers, which is to be expected, considering that the local and diagonal approximation for the diffusion kernel leads to the SSSV theory for the intermediate scattering function.

The difference in the transient site distribution function from the equilibrium one is shown for pNA in Fig. 9. The in-plane distributions of the O- and H-atoms are shown separately as contour plots. The large reorganization of the distribution of the H-atom is observed around the nitro group (as demonstrated earlier, see Fig. 4). It is assigned to the decrease in the strength of the hydrogen bond between the H-atom of water and the nitro oxygen of pNA. An interesting point is that the excess distribution of the O-atom around the nitro group is also positive at $t = +0$ fs, which means that the reorganization of the solvation structure around the nitro group possesses a translational nature. The strong contact distribution of the H-atom around the nitro group decreases from $t = +0$ fs to 100 fs, whereas the diffuse distribution of the O-atom slightly increases. This may be ascribed to the

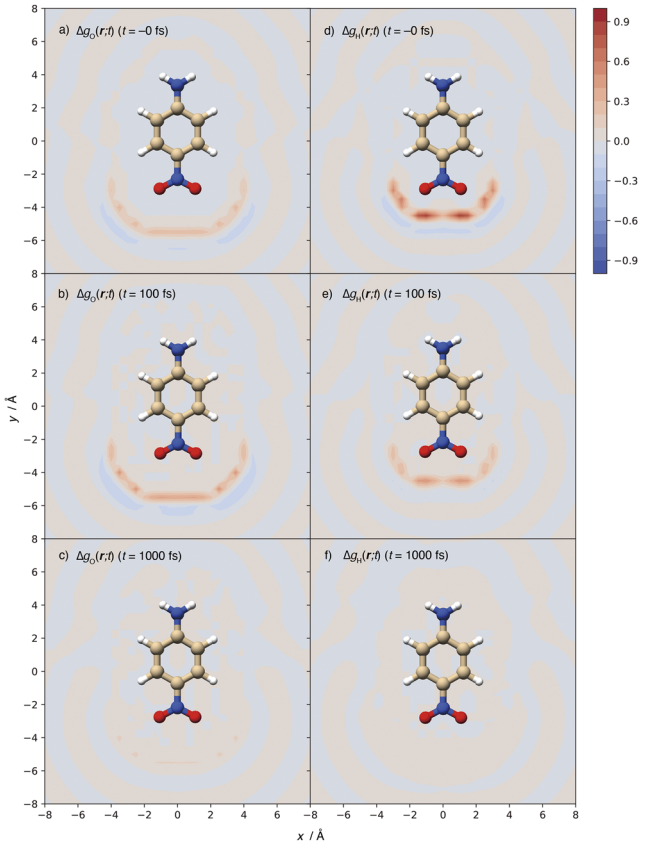

FIG. 9. Difference in the transient site distribution functions around pNA from the equilibrium distribution in the excited state, $g_v(\boldsymbol{r}, t) - g_v(\boldsymbol{r}, t = \infty)$. The in-plane distributions of the O- and H-atoms are plotted in panels (a)–(c) and (d)–(f), respectively. The values of time are +0 fs [(a) and (d)], 100 fs [(b) and (e)], and 1000 fs [(c) and (f)].

reorientation of water in contact with the nitro group. The remaining positive distributions of both atoms relax through the slow mode after 100 fs. The fast and the slow modes of the solvation dynamics of pNA are also assigned to the reorientation and the translation of water, as in the case of the Na atom. The reason for the larger relative amplitude of the slower mode compared with that of the Na atom is that the reorganization of the solvation structure of pNA possesses larger translational character, as shown in Fig. 9.

E. Relaxation path along the nonequilibrium free energy profile

A charge-transfer reaction in solution occurs under the dynamic fluctuation of the solvent, which is described as the motion along the solvation coordinate. The solvation coordinate is a collective dynamic mode of the solvent. The transition energy between the reactant and the product states is often employed as the solvation coordinate. In our previous study, we calculated the nonequilibrium free energy profile along the solvation coordinate.[21] In the present study, the time profiles of the transition energy and the transient free energy are evaluated. Since solvation dynamics is regarded as the collective dynamics along the solvation coordinate, the relationship between $\Delta E(t)$ and $\mathcal{F}(t)$ is expected to follow the nonequilibrium free energy profile if the relaxation of the solvation structure proceeds along the minimum free energy path.

The relaxation paths obtained by our present TDDFT calculation are compared with the nonequilibrium free energy profiles in Fig. 10. In both systems, the transient free energy is slightly higher than that of the nonequilibrium free energy profile. The relaxation paths comprise two parabolas, which are assigned to the faster and the slower modes, respectively. The second parabola is small in the Na atom case, whereas it is approximately as large as the first parabola in the pNA case, which corresponds to the larger relative amplitude of the slower mode of pNA, as shown in Fig. 1. These characteristics are qualitatively the same for systems without inclusion of the electronic polarization of the solvent.

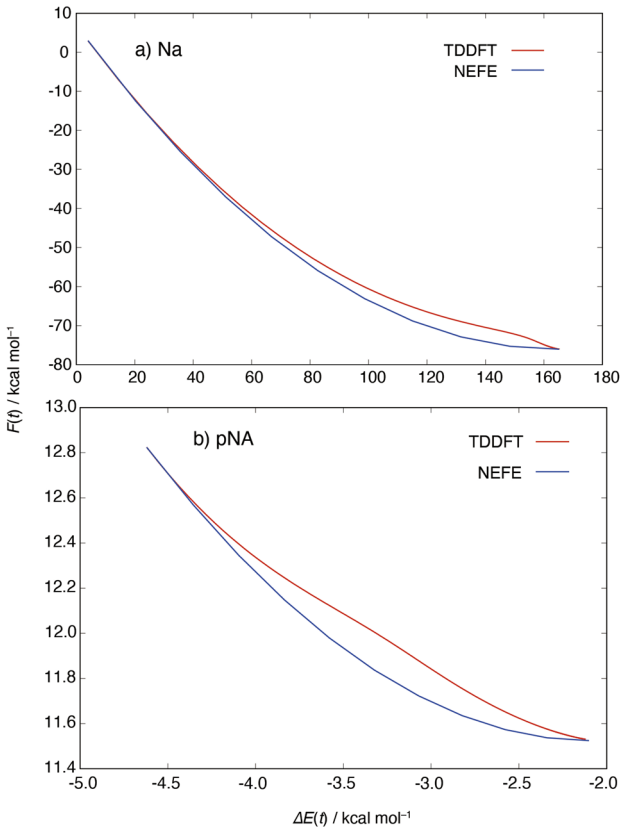

FIG. 10. Relationships between $\Delta E(t)$ and $\mathcal{F}(t)$ of the (a) Na atom and (b) pNA in water. The results of TDDFT calculation in this study are plotted with the red curves, while the nonequilibrium free energy profiles are shown with the blue curves. The left and the right ends of the curves represent the initial and the final equilibrium states, respectively, and the relaxation proceeds from the left to the right.

The deviation of the relaxation path from the nonequilibrium free energy profile can be explained in the following way. The fast and the slow relaxation modes of the solvation dynamics are assigned to the reorientation within the first solvation shell and the long-range translational diffusion. The nonequilibrium free energy profile is the relaxation path on which both the reorientational and the translational modes relax simultaneously. In the solvation dynamics, on the other hand, the translational mode is almost frozen during the fast reorientational relaxation. Therefore, the relaxation must take a path whose free energy is higher than the minimum free energy path. On completion of the reorientational relaxation, the translational mode decays toward the stable equilibrium state.

F. Future perspective

Based on the combination of the sp-3D-RISM theory with TDDFT, we proposed an analytical theory to calculate the time-dependent 3D distribution of the polarization charge density of an electronically polarizable molecular solvent around a solute. The theory was then applied to two model systems. The numerical results that were obtained were physically reasonable.

However, our approximation for the diffusion kernel, the local and the diagonal one, is quite primitive, and some important physics of solvation dynamics might have been lost. First, the inertial nature of the initial dynamics is not captured by the present theory because of the diffusive approximation.[41] Second, the momentum density does not behave as a conserved quantity, which then affects the long-range and long-time dynamics of the translational mode.[42] Third, memory effects on the collective dynamics of the solvent, especially on the reorientational mode of water, are not included.[29]

These weak points are common to the surrogate theory coupled with the SSSV theory because our present theory reduces to SSSV theory when it is applied to the linear fluctuation of the bulk solvent. In the case of the intermediate scattering function of the bulk solvent, the replacement of the SSSV theory by the mode-coupling theory (MCT) can overcome these problems.[43,44] In MCT, the inertial dynamics is captured by treating the momentum density as an explicit variable. The memory kernel on the translational momentum density is proportional to the square of the wavevector in the low-wavevector limit. The slow memory is described as the bilinear form of the intermediate scattering functions. The combination of the surrogate theory with MCT has already been proposed by Nishiyama and co-workers; they obtained improved numerical results of solvation dynamics in molecular solvents.[45] Therefore, the combination with MCT would be a possible route to improve the description of the collective dynamics of the solvent in our theory.

Another possible improvement is the inclusion of the electronic polarizability of the solute. The electronic polarization of the solute, in addition to that of the solvent, is known to affect the nonequilibrium free energy profile of a charge-transfer reaction.[46,47] The conventional 3D-RISM theory has been employed as a tool to treat the solvent effects in quantum chemical calculations—then referred to as the "3D-RISM-SCF theory."[13,48–50] The combination of our sp-3D-RISM theory with quantum chemical calculations is now in progress, within our group, to include the solvation through the electronic polarization of the solvent into the 3D-RISM-SCF theory. The electronic polarization of the solute induced by the reaction field from the solvent is automatically included in the 3D-RISM-SCF theory. The calculation of the electronic structure of the solute at each time step of the dynamics calculation will make it possible to describe the relaxation of the electronic polarization of the solute. The calculation of the transient electronic structure has already been performed by Ishida and co-workers using a combination of RISM-SCF, surrogate, and SSSV theories,[51] and the use of TDDFT instead of the surrogate and the SSSV theories will improve the description of the solvation structure because it can prevent the penetration of the solvent distribution into the repulsive core of the solute during the time development of the solvation structure.[52]

V. CONCLUDING REMARKS

The sp-3D-RISM theory of the solvation structure in electronically polarizable molecular solvents was extended to dynamics through the combination with TDDFT for molecular liquids proposed by Yoshimori.[18] With the simplest approximation for the diffusion kernel, we performed some numerical calculations on the solvation dynamics of representative solutes in water. We obtained detailed information on the transient 3D distributions of the site density and the polarization charge density around the solute during the time course of the solvation dynamics.

The obtained numerical results were considered to be physically reasonable. The relaxation of the transition energy was bimodal; the faster and the slower modes were assigned to the reorientation within the first solvation shell and the long-range translational diffusion, respectively. These assignments are consistent with those proposed by Nishiyama and co-workers based on the surrogate theory coupled with the SSSV theory.[38] The relative amplitude of the slower mode of pNA was larger than that of the Na atom. This was ascribed to the larger coupling of the former with the translational mode.

Upon comparing the solvation dynamics with and without the electronic polarization of the solvent, we found that the relaxation dynamics in the electronically polarizable solvent was slower than that in the nonpolarizable solvent (10%–20% slower). The retardation was then addressed in terms of the longitudinal dielectric relaxation time and the curvature of the nonequilibrium free energy profile along the solvation coordinate.

The relaxation paths in the $\Delta E(t)$–$\mathcal{F}(t)$ plane were calculated for both Na and pNA systems, which is an advantage of our TDDFT-based theory over MD simulation. Although the relaxation path was close to the nonequilibrium free energy profile, a small deviation was found in both model systems. The deviation was then explained in terms of the bimodal character of the relaxation. Since the slow translational mode is frozen during the fast reorientational relaxation, the fast mode must proceed along the path whose free energy is higher than the free energy profile on which both modes are fully relaxed for intermediate states.

Although our present study was limited to numerical calculations on simple model systems, for demonstration, we are planning

to apply the theory to more complicated systems of chemical or biophysical importance.[53,54] In addition, improvement of the theory as discussed in Sec. IV F is also in our future plans.

SUPPLEMENTARY MATERIAL

The numerical algorithm to solve the time development of the site distribution functions is described in the supplementary material.

ACKNOWLEDGMENTS

We acknowledge financial support from the JSPS KAKENHI (Grant Nos. 19H02677 and 19K03768). Numerical calculations were conducted, in part, at the Research Center for Computational Science, Institute for Molecular Science, National Institutes of Natural Sciences. Molecular graphics were depicted with UCSF Chimera, developed by the Resource for Biocomputing, Visualization, and Informatics at the University of California, San Francisco.[55]

DATA AVAILABILITY

The data that support the findings of this study are available from the corresponding author upon reasonable request.

REFERENCES

[1] B. Bagchi and R. Biswas, Adv. Chem. Phys. **109**, 207–433 (1999).
[2] M. Maroncelli, J. Macinnis, and G. R. Fleming, Science **243**(4899), 1674–1681 (1989).
[3] B. Bagchi, Annu. Rev. Phys. Chem. **40**(1), 115–141 (1989).
[4] B. Bagchi, D. W. Oxtoby, and G. R. Fleming, Chem. Phys. **86**(3), 257–267 (1984).
[5] M. Maroncelli, J. Mol. Liq. **57**, 1–37 (1993).
[6] G. Van der Zwan and J. T. Hynes, J. Phys. Chem. **89**(20), 4181–4188 (1985).
[7] S. J. Rosenthal, X. Xie, M. Du, and G. R. Fleming, J. Chem. Phys. **95**(6), 4715–4718 (1991).
[8] K. Nishiyama and T. Okada, J. Phys. Chem. A **102**(48), 9729–9733 (1998).
[9] M. Cho, J.-Y. Yu, T. Joo, Y. Nagasawa, S. A. Passino, and G. R. Fleming, J. Phys. Chem. **100**(29), 11944–11953 (1996).
[10] M. Maroncelli, J. Chem. Phys. **94**(3), 2084–2103 (1991).
[11] T. Yamaguchi, N. Yoshida, and K. Nishiyama, J. Phys. Chem. B **123**(32), 7036–7042 (2019).
[12] J.-P. Hansen and I. R. McDonald, *Theory of Simple Liquids*, 2nd ed. (Academic Press, London, 1986).
[13] F. Hirata, *Molecular Theory of Solvation* (Kluwer, Dordrecht, 2003).
[14] F. O. Raineri, H. Resat, B. C. Perng, F. Hirata, and H. L. Friedman, J. Chem. Phys. **100**(2), 1477–1491 (1994).
[15] F. Hirata, T. Munakata, F. Raineri, and H. L. Friedman, J. Mol. Liq. **65-66**, 15–22 (1995).
[16] H. L. Friedman, F. O. Raineri, F. Hirata, and B.-C. Perng, J. Stat. Phys. **78**(1-2), 239–266 (1995).
[17] A. Chandra and B. Bagchi, J. Chem. Phys. **91**(3), 1829–1842 (1989).
[18] A. Yoshimori, J. Chem. Phys. **105**(14), 5971–5978 (1996).
[19] A. Yoshimori, J. Phys. Soc. Jpn. **80**(3), 034801 (2011).
[20] N. Yoshida and T. Yamaguchi, J. Chem. Phys. **152**(11), 114108 (2020).
[21] T. Yamaguchi and N. Yoshida, J. Chem. Phys. **153**(3), 034502 (2020).
[22] S. J. Singer and D. Chandler, Mol. Phys. **55**(3), 621–625 (1985).
[23] K. Kasahara and H. Sato, J. Comput. Chem. **39**(20), 1491–1497 (2018).
[24] K. Kasahara and H. Sato, J. Chem. Phys. **145**(19), 194502 (2016).
[25] A. Morita and S. Kato, J. Am. Chem. Soc. **119**(17), 4021–4032 (1997).
[26] A. Morita and S. Kato, J. Chem. Phys. **108**(16), 6809–6818 (1998).
[27] F. Hirata, J. Chem. Phys. **96**(6), 4619–4624 (1992).
[28] S.-H. Chong and F. Hirata, J. Chem. Phys. **111**(7), 3083–3094 (1999).
[29] T. Yamaguchi and F. Hirata, J. Chem. Phys. **117**(5), 2216–2224 (2002).
[30] K. R. Harris and L. A. Woolf, J. Chem. Soc., Faraday Trans. 1 **76**, 377–385 (1980).
[31] Y. Kimura, S. Ibaraki, R. Hirano, Y. Sugita, Y. Yasaka, and M. Ueno, Phys. Chem. Chem. Phys. **19**(33), 22161–22168 (2017).
[32] S. A. Kovalenko, R. Schanz, V. M. Farztdinov, H. Hennig, and N. P. Ernsting, Chem. Phys. Lett. **323**(3-4), 312–322 (2000).
[33] P. K. Ghorai and D. V. Matyushov, J. Phys. Chem. B **110**(4), 1866–1871 (2006).
[34] K. Naka, A. Morita, and S. Kato, J. Chem. Phys. **111**(2), 481–491 (1999).
[35] J. S. Perkyns and B. M. Pettitt, Chem. Phys. Lett. **190**(6), 626–630 (1992).
[36] J. Perkyns and B. M. Pettitt, J. Chem. Phys. **97**(10), 7656–7666 (1992).
[37] N. Yoshida, IOP Conf. Ser.: Mater. Sci. Eng. **773**, 012062 (2020).
[38] K. Nishiyama, F. Hirata, and T. Okada, J. Chem. Phys. **118**(5), 2279–2285 (2003).
[39] S. Roy and B. Bagchi, J. Chem. Phys. **99**(12), 9938–9943 (1993).
[40] K. Kasahara and H. Sato, Phys. Chem. Chem. Phys. **19**(41), 27917–27929 (2017).
[41] R. Rey and J. T. Hynes, J. Phys. Chem. B **124**(35), 7668–7681 (2020).
[42] T. Yamaguchi, Y. Kimura, and N. Hirota, J. Chem. Phys. **111**(9), 4169–4185 (1999).
[43] S.-H. Chong and F. Hirata, Phys. Rev. E **58**(5), 6188–6198 (1998).
[44] S. H. Chong and W. Gotze, Phys. Rev. E **65**(4), 041503 (2002).
[45] K. Nishiyama, T. Yamaguchi, and F. Hirata, J. Phys. Chem. B **113**(9), 2800–2804 (2009).
[46] S. Gupta and D. V. Matyushov, J. Phys. Chem. A **108**(11), 2087–2096 (2004).
[47] D. W. Small, D. V. Matyushov, and G. A. Voth, J. Am. Chem. Soc. **125**(24), 7470–7478 (2003).
[48] H. Sato, A. Kovalenko, and F. Hirata, J. Chem. Phys. **112**(21), 9463–9468 (2000).
[49] A. Kovalenko and F. Hirata, J. Chem. Phys. **110**(20), 10095–10112 (1999).
[50] S. Ten-No, F. Hirata, and S. Kato, J. Chem. Phys. **100**(10), 7443–7453 (1994).
[51] T. Ishida, F. Hirata, and S. Kato, J. Chem. Phys. **110**(23), 11423–11432 (1999).
[52] T. Ishida, J. Phys. Chem. B **113**(27), 9255–9264 (2009).
[53] S. Mukherjee, S. Mondal, S. Acharya, and B. Bagchi, J. Phys. Chem. B **122**(49), 11743–11761 (2018).
[54] J. Ma, A. Kumar, Y. Muroya, S. Yamashita, T. Sakurai, S. A. Denisov, M. D. Sevilla, A. Adhikary, S. Seki, and M. Mostafavi, Nat. Commun. **10**(1), 102 (2019).
[55] E. F. Pettersen, T. D. Goddard, C. C. Huang, G. S. Couch, D. M. Greenblatt, E. C. Meng, and T. E. Ferrin, J. Comput. Chem. **25**(13), 1605–1612 (2004).